Water desalination by capacitive electrodialysis: experiments and modelling

A. Campione[a], A. Cipollina[a,], E. Toet[b], L. Gurreri[a], I. D. L. Bogle[c], G. Micale[a]*

[a] *Dipartimento di Ingengeria, Università degli Studi di Palermo, viale delle Scienze Ed.6, 90128 Palermo, Italy*

[b] *FUJIFILM Manufacturing Europe, Oudenstaart 1, 5000 LJ Tilburg, The Netherlands.*

[c]*Centre for Process Systems Engineering, Department of Chemical Engineering, University College London, Torrington Place, London WC1E 7JE, UK.*

[*]*Corresponding Author (A. Cipollina):* andrea.cipollina@unipa.it

Abstract

Electrodialysis-related technologies keep spreading in multiple fields, among which water desalination still plays a major role. A yet not thoroughly investigated technology is represented by capacitive electrodialysis (CED), which couples the standard ED with the concept of capacitive electrodes. CED is connected to a number of advantages such as removal of toxic products and system simplification. Only little mention is made of this technology in the literature and, to the best of our knowledge, no modelling works have ever been presented. Therefore, in this work, the CED process has been studied through experiments and modelling. A CED model, based on a hierarchical structure, has been presented for the first time. Upon a simple calibration based on macroscopic membrane properties and the characterisation of electrodes behaviour, the model is able to simulate the dynamics of simple as well as more complex layouts where one or more CED units are involved. An original experimental characterisation of electrodes is presented, showing how the collected data can be implemented into the model. After a successful validation with experimental data, dynamic simulations of a single pass CED unit have been performed with the aim of assessing the effect of

different capacitive electrodes properties on process performance. Results showed how the impact of these properties is different depending on the number of cell pairs chosen for the unit.

Keywords: *Dynamic simulation, desalination, ion exchange membrane, electromembrane process, carbon electrode.*

1. Introduction

Electrodialysis (ED) is an electrochemical process that involves the use of ion exchange membranes that are able to selectively orient the motion of either anions or cations [1,2]. The ED unit, often referred as stack, is generally based on a plate and frame arrangement, where cation and anion exchange membranes (AEMs and CEMs) are alternatively arranged in series. Channels for water flow are formed in between membranes by separators (i.e. spacers) giving mechanical stability to the channels and promoting mixing [2]. In particular, an AEM, a CEM and two adjacent channels form the repetitive unit, referred as the cell pair (Figure 1). Finally, the device is closed with two end plates.

Upon application of an electric potential, anions and cations start to move in opposite directions. As a result of the alternated presence of CEMs and AEMs, cations will be able to flow through the former, while they will be almost totally blocked by anionic membranes. Conversely, anions will preferentially pass through AEMs. Therefore, ions (and thus salt) can be removed from one channel (referred as the diluate), while being accumulated in the adjacent one (i.e. the concentrate) producing the desalted product as well as a concentrate by-product. In a typical ED stack, current flow is ensured by the presence of faradaic electrodes that are mounted onto the endplates and are connected to a power supply. Therefore, the two end channels (the ones created in between the endplate and the last membrane in each side) are devoted to the circulation of an electrode rinse solution allowing the charge transfer by redox reactions that convert the electronic flux in the external circuit into the ion flux inside the stack. Usually, NaCl or Na_2SO_4 [3,4] are selected as electrolytes.

Capacitive electrodes represent a promising alternative to conventional electrode systems and have been recently proposed in applications for ED and reverse ED [5–7]. Porous capacitive electrodes act as a mean of current transport by physico-chemical mechanisms of adsorption and desorption of ions (thus ejecting/capturing electrons) instead promoting electrochemical reactions (Figure 1). There are a number of advantages associated with the use of capacitive electrodes such as the absence of unstable or toxic products (i.e. Cl_2, O_2 and acids or bases, depending on the electrode solution adopted), the reduction of the electrodic potential drop. In addition, system complexity is reduced due to the absence of the hydraulic circuit that in standard ED is used to recirculate the electrode rinse solution [5,7]. On the other hand, capacitive electrodes suffer from saturation of the carbon layer due to charge accumulation, so that the electrical polarity (as well as concentrate and diluate compartments) needs to be periodically switched in order to operate the desalination process for a long time. However, this drawback is compensated by the fact that ED plants usually operates in ED reversal mode, where a periodical polarity switch is already adopted to address membrane fouling issues. Therefore, such systems are already suitable for the use of capacitive electrodes.

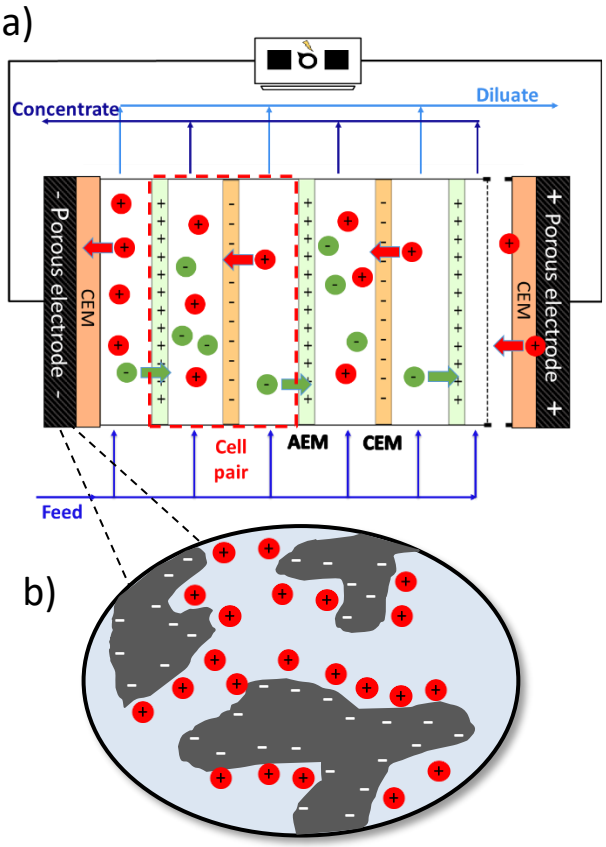

Figure 1. a) Schematic representation of the electrodialysis process with capacitive electrodes (CED), b) detail on the porous structure of the capacitive electrode.

Although a lot of complex phenomena can be involved [8,9], in principle a capacitive electrode is able to store charges in the form of ions through formation of the electric double layer (EDL) upon electrical polarisation [8,10]. As the EDL is formed on the pores surface, the higher the specific area, the higher the amount of ions that can be stored/released. Therefore, it is imperative to use materials with high surface area in order to avoid too frequent polarity switches. A good conductivity is also desirable, in order to limit the Ohmic losses at the electrodes. For this reason, capacitive electrodes are mainly made by carbon materials [8], although alternatives such as conductive polymers have been also investigated [11]. Among the carbon materials, different authors have reported the use of graphene with various structures, such as aerogels [12] multi-layer nanoribbons [13,14], nanotubes [12,15–18] and carbon onions [18,19]. In particular, Portet et al. [18] showed how onions are specifically suitable for energy storage applications, due to their ability to rapidly deliver charges. Another good material is carbon black, which is able to provide a high surface area (> 1500 m^2/g)

through agglomeration of nanoparticles [8,20]. However, the most common electrodes are usually made by activated carbons, characterised by randomly oriented and highly cross-linked graphene layers [21–28]. Activated carbons are particularly attractive as they combine high surface area with low production costs, as they can be produced by natural precursors such as fruit stones [28], leaves [21] and pitch [29].

The ability of capacitive electrodes of storing and delivery ionic charges made them suitable for two fields: conversion and storage of energy and desalination. In the first one, supercapacitors represent by far the most common application [30,31], although there are some other processes such as Reverse ED (RED) with capacitive electrodes [7] or with capacitive flow electrodes [32], capacitive cell with CO_2 solutions [33], capacitive double-layer expansion [34] and other CAPMIX technologies [8]. Among the desalination technologies, capacitive electrodes are mostly acknowledged for the capacitive deionisation process [35–39].

Although carbon electrodes have been being thoroughly studied and applied to many processes, to the best of our knowledge only few mention of electrodialysis with capacitive electrodes (CED) is made in the literature [5,6]. In addition, no CED modelling works have been published yet. In this work, the CED process has been thoroughly studied by means of modelling and experiments. A set of galvanostatic experiments on a lab scale CED stack has been performed with the aim of testing the process desalination capability and characterising a set of capacitive electrodes. In addition, a CED process model has been presented for the first time. The modelling tool has been implemented by a hierarchical approach that simulates the main dynamic phenomena involved in the CED process and ensures high flexibility in simulating different scales and layouts, ranging from the simple single pass lab-unit up to complex multistage industrial installations. After a model validation by means of the aforementioned experimental data, simulations have been performed in order to present the predictive capability of the modelling tool and analyse the process performance under a variety of operating conditions.

2. Modelling state of the art

Despite the lack of published CED models, there are a lot of modelling works either on ED [40–53] or on capacitive electrodes applied to other processes [9,54–60].

Many approaches can be adopted to build an ED model, ranging from simplistic to more rigorous ones. [2]. Among all the possible approaches, semi-empirical models represent a good balance, as an extensive description of non-ideal phenomena is provided requiring only easily measurable quantities as input parameters (e.g. macroscopic membrane properties). This method has already been presented for both RED [61–63], and ED [45,64–67].

Capacitive electrodes have been extensively modelled at different scales within the context of different applications. In the most basic approach, the electrode is represented by a simple electrical circuit composed by a capacitor and a resistor (*RC circuit model*) [54,55]. Although this approach does not take into account the physical structure of the carbon material, all the electrode characteristics are condensed into the values of the two electrical elements that are relatively easy to measure. Therefore, this simple yet effective approach is particularly useful for process models, as it requires only few easily accessible information.

A more detailed approach to the problem is represented by the *transmission line model* [10,55,68,69]**.** In this case, the porous electrode structure is approximated through a complex circuit with electrical elements (i.e. resistor, capacitors and impedances) arranged in series and parallel. Different degrees of complexity can be found based on the assumed porous structures, ranging from simple RC transmission lines [68,69] up to a complex arrangement of hierarchical impedances when a bimodal porous structure has to be described [10]. This type of models can be calibrated on a specific capacitive electrode by quantifying a set of fitting parameters in the form of electrical elements by means of electrical impedance spectroscopy measurements [10].

A completely different approach is based on the theoretical description of the EDL. Traditionally, models belonging to this category are based on the Gouy-Chapman-Stern theory [9,57,58]. Alternatively, the Donnan and modified Donnan models provide a more comprehensive description, involving the dynamics of EDL formation and accounting for overlapping EDLs typical of small pores [56,60,70,71]. The latter class of models can also be extended to account for non-electrostatic ion adsorption [56] and faradic reactions [60]. Theoretical models for capacitive electrodes can predict electric potential distributions inside the pores. However, complex and controversial parameters, such as the capacitance of micropores [56] need to be estimated.

In the CED model developed in this work, an existing semi-empirical hierarchical ED model [67] has been properly modified and extended to account for the presence of capacitive electrodes, which have been modelled by means of a distributed RC circuit.

3. Model

A dynamic CED hierarchical model has been developed. The starting point for the current formulation is a pre-existing steady-state ED one-dimensional process simulator [67] that has been adapted for the purpose of accounting for the peculiarities of the new process. Consequently, existing hierarchies have been modified to take into account the intrinsic dynamic behaviour, considering all the variables being also function of time (Figure 2).

Starting from the lowest scale, the model simulates mass transport and electrical behaviour of the cell pair (i.e. the ED repeating unit) and the capacitive electrodes. These two instances have been coupled in the second level where the whole stack is modelled (Figure 2 c). Finally, the stack model has been implemented in the plant model, i.e. the highest scale that can simulate different process layouts (i.e. single stage, multistage, batch, feed and bleed etc.).

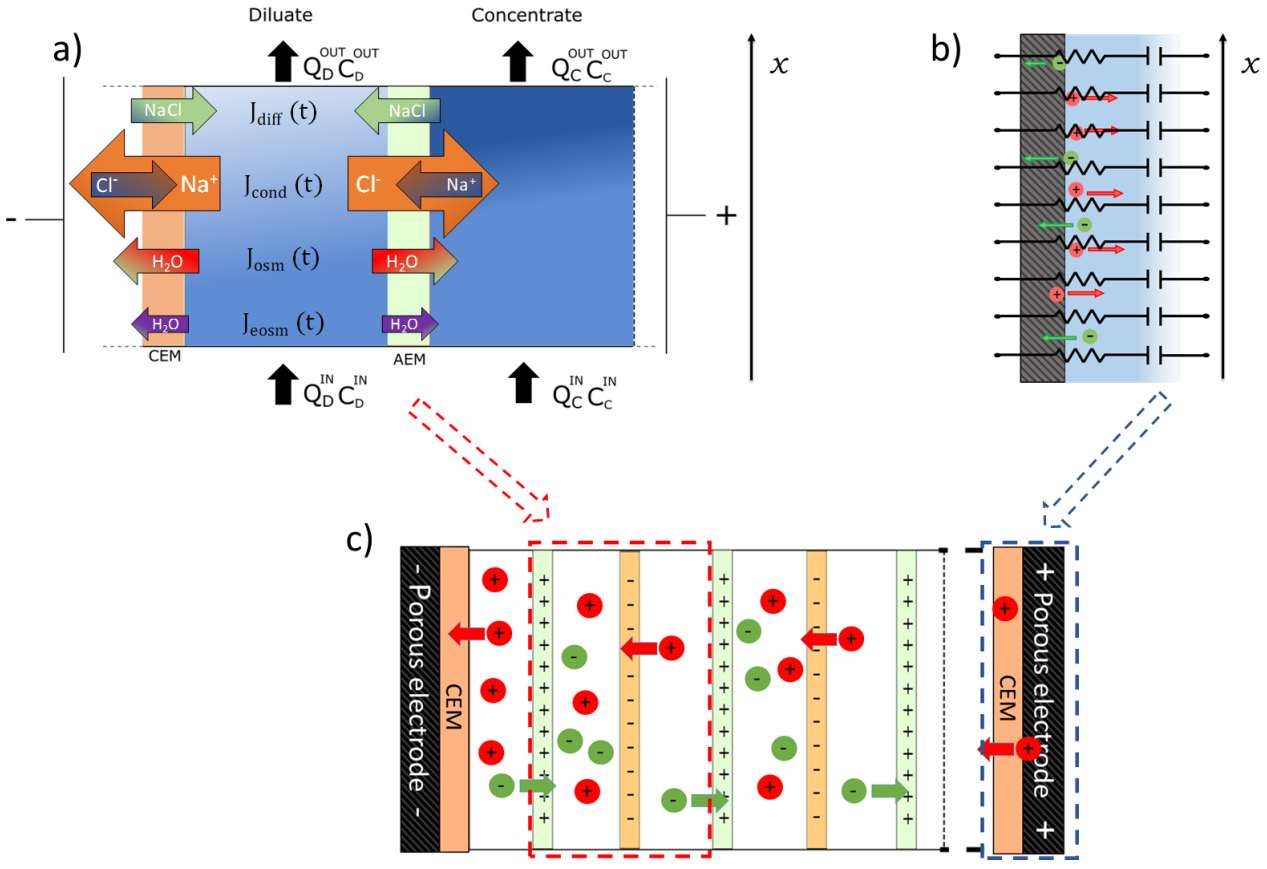

Figure 2. Schematic representation of the model hierarchies. a) Cell pair, b) capacitive electrode, c) stack.

3.1 Capacitive electrodes model

Each capacitive electrode has been modelled as a distributed entity, thus being divided into a number of discretisation intervals in the direction of the channel length (Figure 2 b). A simple RC circuit has been used to model the behaviour of each interval. No contributions for unwanted faradic reactions or non-electrostatic adsorption have been considered. Therefore, the time-dependent distributed electrode voltage drop (ΔV_{el}) can be written as:

$$V_{el}^{j}(x,t) = \frac{Q_{el}^{j}(x,t)}{c_{el}^{j}(x,t)} + R_{el}^{j} i(x,t) \tag{1}$$

where Q_{el} is the amount of charge per unit of projected area collected by the capacitor at a given time and position, c_{el} is the electrode capacitance per unit of projected area, R_{el} the electrode areal

resistance, i is the current density and x and t are the space and time coordinates respectively. The superscript j represents the fact that the equation is valid for both of the electrodes in the CED unit. It is worth noting that, considering a spatial distribution, each discretised electrode volume can behave differently from each other, thus potentially having different values of charge, capacitance, resistance and, thus, voltage at every x. This assumption has been done in order to account for the fact that in a real unit the electrode can be subjected to a very different concentration and current density along the channel direction, thus potentially behaving very differently from the inlet to the outlet of the stack.

In this work, the value of c_{el} has been experimentally determined as a function of the solution concentration by means of galvanostatic methods (see section 4).

3.2 Cell pair model

The cell pair model has also distributed parameters and includes salt and water mass balances and transport equations (Figure 2 a), electrical equations and correlations for the estimation of thermodynamic properties of salt solutions and membranes [67]. Table 1 summarises the main equations implemented in the model. For the meaning of all quantities, refer to the list of symbols.

Table 1. List of the main equations for mass transport in the cell pair model.

Described phenomenon	Equation	
Salt mass balance	$A\delta_D \frac{\partial C_{SOL}(x,t)}{\partial t} + \frac{\partial Q_{SOL}(x,t) C_{SOL}(x,t)}{\partial x} = \pm b\, J_{tot}(x,t)$	(2)
Overall diluate mass balance	$\frac{d\, Q_D(x,t)}{dx} = \pm\, b\, q_w(x,t)$	(3)
Conductive salt flux	$J_{cond}(x,t) = [t_{CEM}^{counter} - (1 - t_{AEM}^{counter})] \frac{i\,(x,t)}{F}$	(4)
Diffusive salt flux	$J_{diff}^{IEM}(x,t) = -\frac{D^{IEM}}{\delta^{IEM}} ({C_C}^{int,IEM}(x,t) - {C_D}^{int,IEM}(x,t))$	(5)
Overall salt flux	$J_{tot}(x,t) = J_{cond}(x,t) + J_{diff}^{AEM}(x,t) + J_{diff}^{CEM}(x,t)$	(6)
Osmotic water flux	$q_{osm}^{IEM}(x,t) = L_p^{IEM}\left(\pi_C^{IEM}(x,t) - \pi_D^{IEM}(x,t)\right)$	(7)

Electroosmotic water flux	$q_{eosm}(x,t) = \frac{w\, J_{tot}(x,t) M_w}{\rho_w}$	(8)
Overall water flux	$q_w(x,t) = q_{osm}^{AEM}(x,t) + q_{osm}^{CEM}(x,t) + q_{eosm}(x,t)$	(9)

Differently from the original steady-state model, most of the variables are now intrinsically functions of time (t) as well as space (x) and salt material balances (eq.(2)) have the time derivative term.

The cell pair electrical terms have also been computed at this scale. Interestingly, due to the discretisation of the capacitive electrodes (whose model is coupled with the cell pair model at the stack level), it is not possible to define a single voltage drop over a cell pair (ΔV_{cp}) independent from the spatial coordinate. In fact, only in the stack, where current collectors impose an equipotential surface, it is possible to define a unique value of the voltage (for more details, see section 3.3). Therefore, ΔV_{cp} is different for each single branch of the cell pair equivalent electrical circuit, thus becoming a function of x. According to the cell pair equivalent circuit (depicted between the brackets in Figure 3):

$$V_{cp}(x,t) = \eta\,(x,t) + R_{tot}(x,t) i(x,t) \quad (10)$$

where η is the non-Ohmic voltage drop associated to the back electromotive force where concentration polarisation is also taken into account making use of computationally determined Sherwood numbers [67,72–74] and R_{tot} is the total areal Ohmic resistance of cell pair that can be calculated as the sum of membranes and solution compartments resistances [67].

3.3 Stack model

The stack model simulates a series of cell pairs between two capacitive electrodes, which are positively or negatively polarised. Within the stack, it is possible to compute power consumption, performance parameters and overall quantities such as the applied voltage [67]. At a given time,

performance parameters are defined as in the classical ED process, while the external applied voltage (ΔV_{tot}) can be calculated by summing up the voltage drop of all cell pairs and of the two electrodes at any position (according to the system equivalent circuit shown in Figure 3):

$$V_{tot}(t) = \left(\sum_{i=1}^{Npairs} \Delta V_{cp_i}(x,t) \right) + \Delta V_{el}^{1}(x,t) + \Delta V_{el}^{2}(x,t) \tag{11}$$

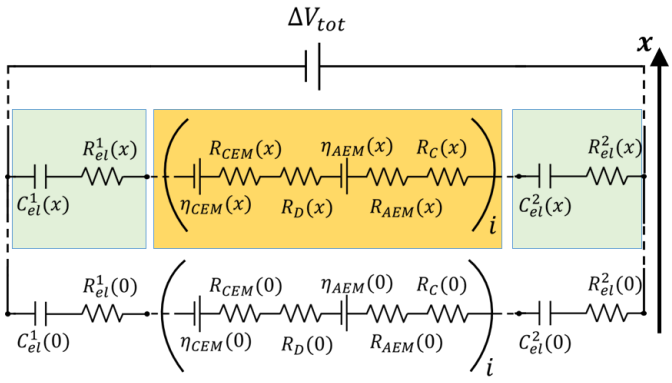

Figure 3. Scheme of the distributed equivalent electrical circuit representative of the stack model, including the cell pair circuit (in brackets) in series with the RC elements of the capacitive electrodes. For the sake of brevity, only the branches that describe the position x = 0 (channel inlet) as well as one for a generic x position have been explicitly represented.

Despite the fact that the voltage of each element (i.e. cell pairs and the two electrodes) can be different at each x position, the total voltage is a single parameter, as it represents the value that can be externally measured at the current collectors.

3.4 Plant model

The plant model represents the highest hierarchy of simulation, where a number of stack models can be variously arranged together with other auxiliary units. In a previous work [67] multistage and batch configurations for standard ED have been assessed highlighting the operating advantages of some possible arrangements. However, also more complex layouts can be simulated, including the presence of recycle streams, typical of feed and bleed configurations.

4. Experimental

A 10×10 cm^2 bench-scale CED unit (*Deukum GmbH, Germany*), equipped with carbon capacitive electrodes with graphite current collectors (*Fujifilm Manufacturing Europe B.V., The Netherlands*), operating in a single pass co-flow arrangement was tested. The stack has been piled with 10 cell pairs made by Type 10 ion exchange membranes (*Fujifilm Manufacturing Europe B.V., The Netherlands*) whose main properties are listed in Table 2, and 270 µm woven spacers (*Deukum GmbH, Germany*) [75]. CEMs end-membranes have been placed in direct contact with the electrodes, so that almost only cations are involved in the formation of EDL at the electrodes. For this reason, during the operation one capacitor will accumulate cations while the other will desorb them. A schematic representation of the stack assembly is provided in Figure 4.

Table 2. Properties of Type 10 Fujifilm membranes (provided by the manufacturer).

Membrane	Thickness δ (µm)	Permselectivity α*	Water permeability L_p (ml/(bar h m^2))	Resistance R (Ω·cm^2)**
AEM	130	0.969	6.29	1.77
CEM	130	0.975	7.79	1.89

*Permselectivity measured in between 0.05M/0.5M KCl solutions

**Membrane resistance measured with 0.5 M NaCl solution

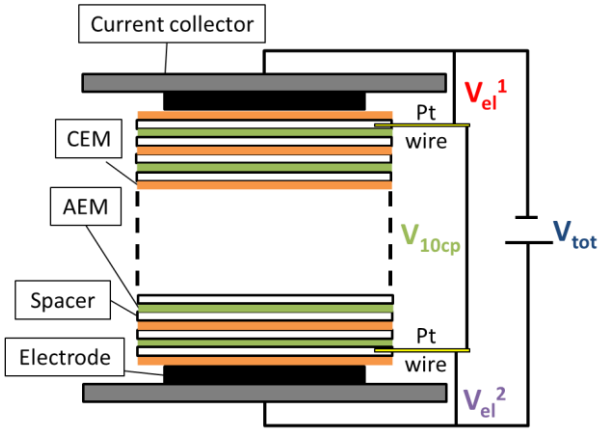

Figure 4. Schematic representation of the CED unit used for the experiments. V_{tot} ,V_{el}^1,V_{el}^2 and V_{10cp} indicates the experimentally measured voltage drops: overall voltage drop (V_{tot}), electrode 1 voltage drop (V_{el}^1), electrode 2 voltage drop (V_{el}^2), cell pairs voltage drop (V_{10cp}).

NaCl solutions at different concentrations (1, 3, 5 and 10 g/l) have been pumped with a flowrate of ~ 490 ml/min (3 cm/s) through the stack using DC controlled diaphragm pumps fed back by flow meters (Krohne, Germany). Solutions conductivity has been measured and continuously monitored both at the inlet and at the outlet through conductivity meters (*HORIBA Ltd., Japan*)

The experiments have been performed under galvanostatic conditions (constant current) by means of a power supply (*Conrad Electronic International GmbH, Germany*). Platinum wires (Agar Scientific Ltd., UK) have been used to measure the voltage drop over the membrane pile excluding the electrodes (V_{10cp}, as shown in Figure 4) and over the single electrodes (V_{el}^1 and V_{el}^2 from Figure 4). Voltages have been continuously measured and recorded through an acquisition system (*Rigol Technologies Inc., U.S.*).

During a single galvanostatic test, a constant current has been maintained for a chosen time period in order to avoid excessive voltage over the electrodes, and thus the occurrence of water splitting. At the end of the period, polarity switch inverted the direction of the fixed current (Figure 5 a). The switches have been repeated for a number of cycles in order to ensure the achievement of a regular periodic operation.

Figure 5 a shows an example of the electrical voltages measured during a typical experiment. Apart from V_{tot}, the graph depicts V_{el}^1, V_{el}^2 and V_{10cp}. It is worth noting that the voltages are always represented as voltage drops (so that $\sum V_i = V_{tot}$). Therefore, when a positive current (orange line) is applied, V_{el}^1 represents the voltage drop of the electrode that is adsorbing cations (and thus acting as a *passive* charging element), while the negative value of V_{el}^2 is representative of the electrode that is actively discharging and thus providing part of the current. The opposite happens when a negative current is applied.

From the V_{tot} *vs* time curves obtained from the experiments, it was possible to estimate the equivalent capacitance of the electrodes by means of the following equation:

$$\frac{dV_{tot}}{dt} = \frac{i}{c_{el}^{eq}} \tag{12}$$

where $\frac{dV_{tot}}{dt}$ is the slope of the overall voltage *vs* time curve (linear parts of V_{tot} curve as in Figure 5 b), i is the overall current and c_{el}^{eq} is the equivalent areal electrode capacitance, accounting for both capacitive electrodes. If the charging (or discharging) voltage curve of the two electrodes is almost equivalent, it can be assumed that their behaviour is the same. Consequently, the capacitance of a single electrode can be taken as twice as the value estimated from eq.(12). In the case of highly asymmetric behaviour (i.e. when two completely different electrodes are used at each side of the CED unit), the capacitance of the each electrode can be also deduced directly from the slope of each V_{el}^{j} voltage curve.

At a given feed concentration (that could be assumed as the concentration inside the stack channels due to the high flowrate), the capacitance has been averaged over each value measured from positive and negative voltage curves. In addition, each experiment has been repeated from 2 to 3 times.

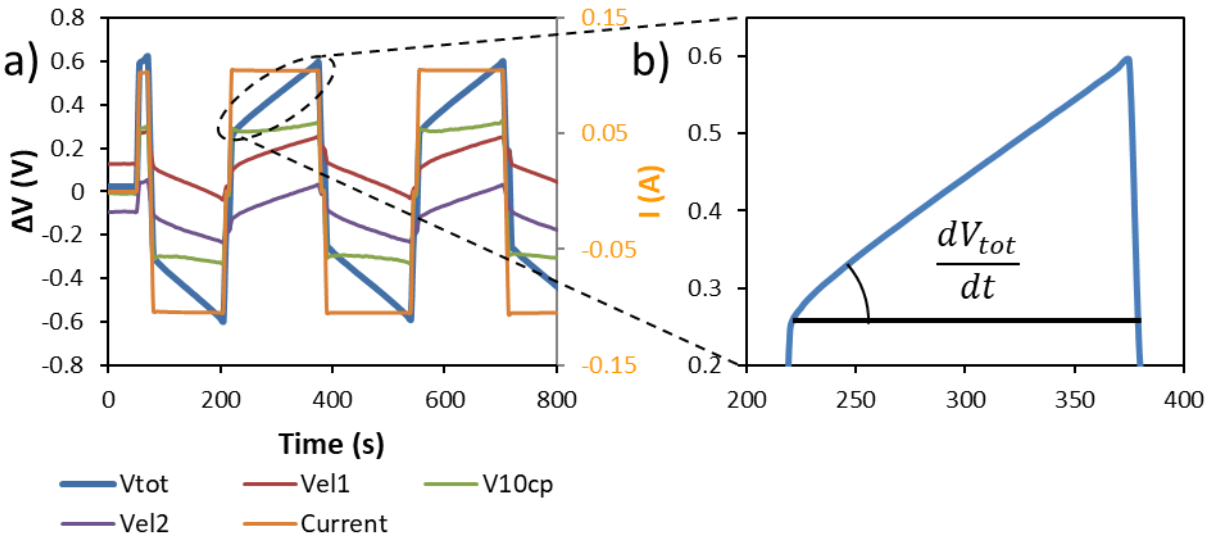

Figure 5. a) Representation of a typical experimental voltage vs time curve showing the overall voltage drop (V_{tot}), electrode 1 voltage drop (V_{el}^{1}), cell pairs voltage drop (V_{10cp}), electrode 2 voltage drop (V_{el}^{2}) and the applied current. b) Detail of a linear part of V_{tot} vs time curve used for the estimation of electrode capacitance. The graphs refer to a 1 g/l feed concentration and ±0.1 A, where positive or negative sign of the current indicates the two different polarities.

5. Results and discussion

In the first part of this section, the results from the experimental capacitance measurements are shown. Then, predictions of the CED process simulations, performed with the experimentally determined values of electrode capacitance, are compared with the experimental data of the CED unit for validation purposes. Finally, simulation results aimed at assessing the influence of capacitive electrode parameters and number of cell pairs on the process performance are presented and discussed.

5.1 Bench-scale CED stack

5.1.1 In-situ experimental characterization of the capacitive electrodes

Figure 6 shows the specific capacitance per cm^2 of projected area estimated from the overall voltage versus time curves (c_{el}^{eq}) as a function of solution concentration. Error bars have been determined from the standard deviation of the outcomes of each repeated experiment. The slightly increasing trend of the capacitance can be explained by the formation of the electric double layer at the nanoscopic scale that is influenced by the amount of ions in the solution, as traditionally formulated by the Gouy-Chapman model of the diffuse EDL [76]. Given the common nature of the two electrodes of this specific unit (see section 4), the capacitance of a single electrode has been taken as twice as the value reported in Figure 6.

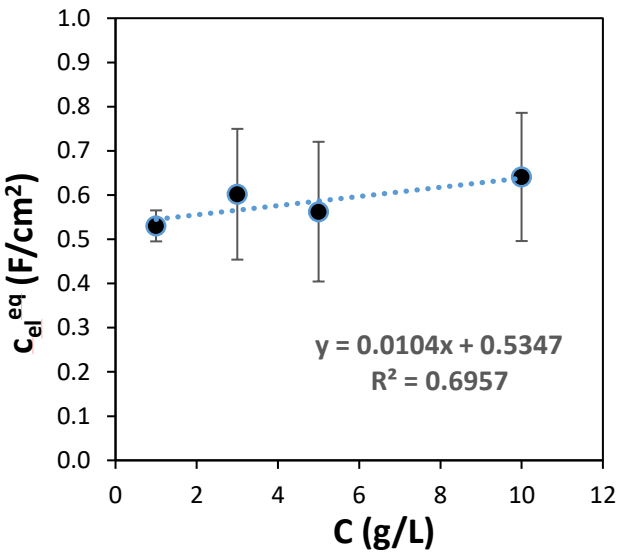

Figure 6. Measured specific overall electrodes capacitance (c_{el}^{eq}) as a function of solution concentration.

5.1.2 Experimental characterization of the CED unit and model validation

The correlation of the capacitance *vs* the concentration obtained from the experimental results has been implemented into the capacitive electrode model of the CED process simulator in order to predict the behaviour of the experimentally characterised electrodes. Therefore, it was possible to assess the model reliability in simulating the operation of the CED unit by comparison with the experimental curves. *gProms Modelbuilde*r (*PSE, UK*) has been used as simulation platform.

Simulations have been performed by applying the electrodes open circuit voltages (i.e. measured when no current was flowing through the system) as initial condition. Those voltages are associated to the fact that a certain amount of charge is already accumulated at the electrode surface. In addition, the value of the electrode ohmic resistance has been calibrated from the instantaneous step voltage response of each electrode when the current is applied (Figure 7 c and Figure 8 c) and ranged from 50 to 100 $\Omega \cdot m^2$, based on solution concentration.

Figure 7 shows simulation results in comparison with the experimental data for the case of 10 g/l feed and ±0.15 A current. As shown, the process is actively desalinating one feed stream while

concentrating the other (Figure 7 d). At a given polarity, the cell pair voltage stays constant as the desalination rate is kept constant by the applied current. On the other hand, the absolute value of V_{el}^{1} and V_{el}^{2} (Figure 7 c) grows in order to maintain the desired current. Interestingly, after the first two cycles the operation is quite stable and able to maintain the same performances for multiple cycles. Therefore, it seems realistic to imagine wider CED stacks (i.e. with larger active area) that can steadily desalinate a feed stream down to the drinking water concentration target.

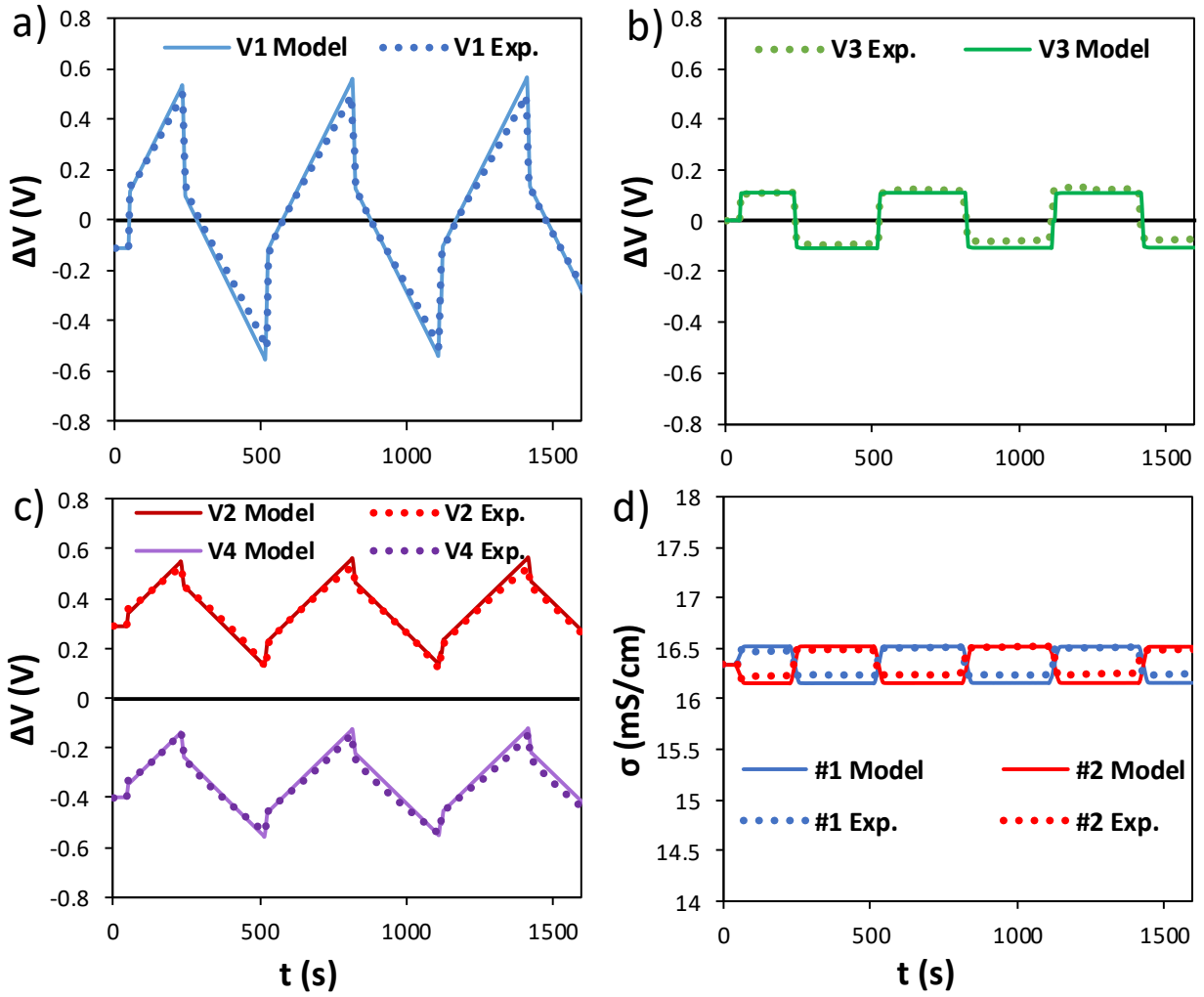

Figure 7. Model predictions compared with experimental data of a bench-scale 10×10 cm² CED stack equipped with 270 µm woven spacers and Type 10 Fujifilm membranes. Inlet concentration of 10 g/l flowrate of 486 ml/min and applied current of ±0.15 A with polarity switches every ~280 s. a) Overall voltage drop, b) Cell pairs voltage drop, c) Electrodes voltage drop, d) outlet conductivity of the two compartments.

Other operating conditions have been tested through both experiments and simulations. For example, Figure 8 shows the case of 1 g/l of salt concentration and ±0.1 A current. Similarly to the previous case, the desalination capability has also been demonstrated for lower concentration feeds. The main difference is that in this case the cell pair voltage drop (Figure 8 b) is much higher due to the lower solution conductivity. Consequently, shorter cycles have been performed in this case, despite the fact that the slope of the total voltage curve (Figure 8 a) is flatter due to the lower applied current.

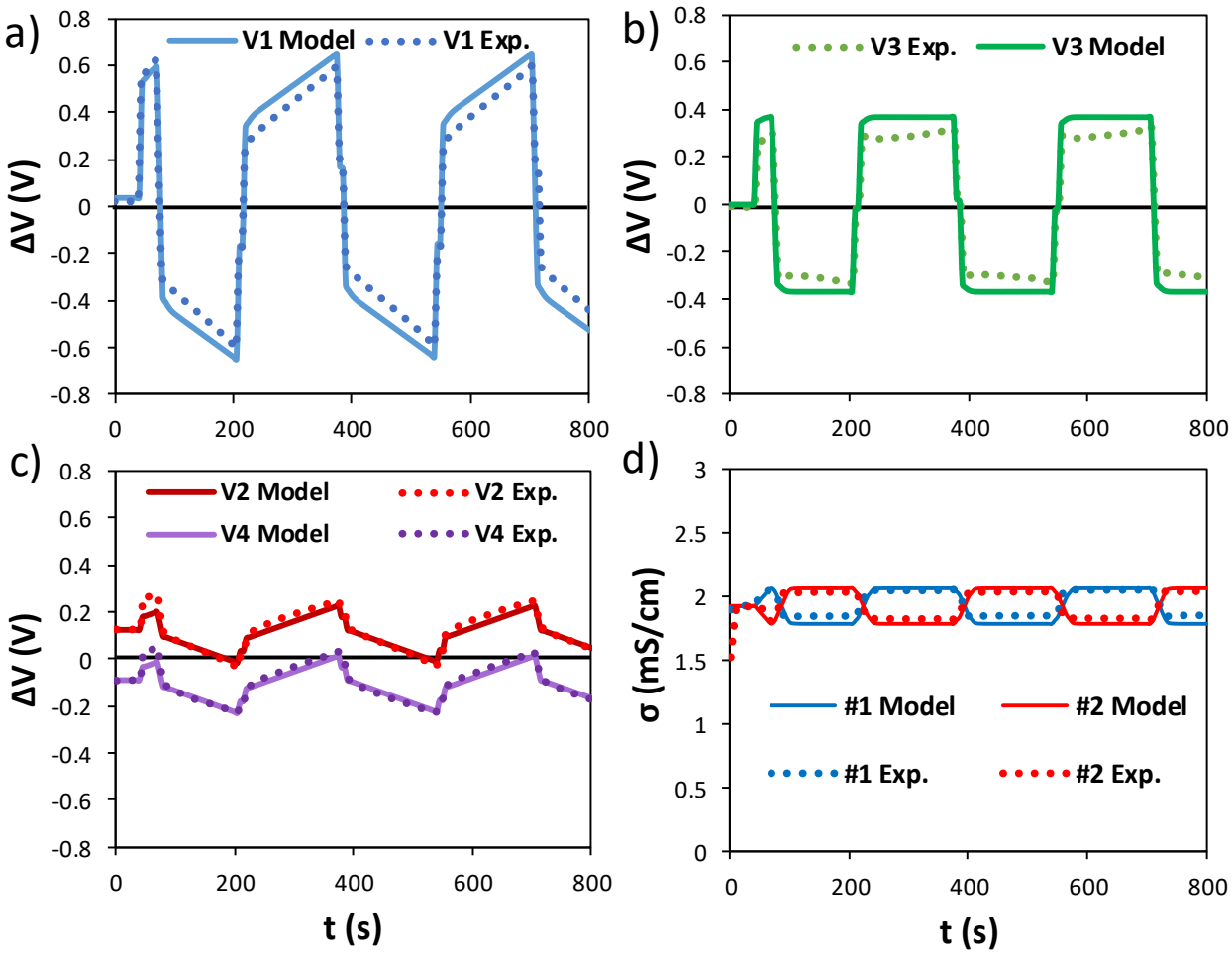

Figure 8. Model predictions compared with experimental data of a 10×10 cm² CED stack equipped with 270 µm woven spacers and Type 10 Fujifilm membranes. Inlet concentration of 1 g/l, flowrate of 486 ml/min and applied current of ±0.1 A with polarity switches every ~180 s. a) Overall voltage drop, b) average cell pairs voltage drop, c) electrodes voltage drop, d) outlet conductivity of the two compartments.

In general, Figure 7 and Figure 8 demonstrates that the model has a good prediction capability in different operating conditions both for the voltage *vs* time curves, as well as for the outlet conductivities. However, the model shows a slight overestimation of the average cell pair voltage drop (Figure 8 b). This discrepancy can be attributed to the stack assembly. According to the scheme of Figure 4, the dimensions of the carbon electrodes are limited to the 10×10 cm^2 active area and no external gaskets are used to compensate the localized increase of thickness that takes place in the central part of the stack. Therefore, when the stack is closed, the electrodes apply a localized pressure on the active area of the membranes that are directly compressed over the spacer netting, reducing the real thickness of the channels and thus the channel Ohmic resistance. For low feed concentrations (as for the 1 g/l case) the resistance is higher and the difference between the real and the nominal value of the resistance enhances the differences between the predicted and the measured voltage values.

5.2 Performance prediction of large-scale CED stacks

In real scenarios, salty water feeds need to be desalted down to drinking water salt concentration. In order to apply the CED technology to those cases, larger units compared to the ones experimentally tested have to be considered. In this context, the model is a suitable tool to analyse the process in wider and more industrial-relevant conditions.

Following the model validation, a single pass CED operation has been simulated for a scaled-up configuration with 12 cell pairs and an active area of 12.5 (width) × 80 (length) cm^2. A resistance of 50 $\Omega \cdot cm^2$ has been attributed to the electrodes (see section 5.1.2). Starting from a reference case, the CED model has been used to assess the effect of the electrode features on the process performances (section 5.3.1 and 5.3.2).

The CED unit had to desalt a 2 g/l NaCl feed solution flowing with a linear velocity of 2 cm/s. This time, potentiostatic operations with a constant voltage of ±2 V have been simulated as this mode of

operation is the most common in commercial applications. Multiple polarity switches have been performed every 10 minutes (600 s). It is worth noting that the chosen switching time is not too far from the usual switching time of EDR plants (between 15 and 30 minutes). In order to simulate the CEM end membrane scheme, the electrode that is accumulating charge during the first cycle has a zero charge initial condition, while the opposite electrode is assumed to be pre-charged with a Q_{el} of 1 C/cm^2.

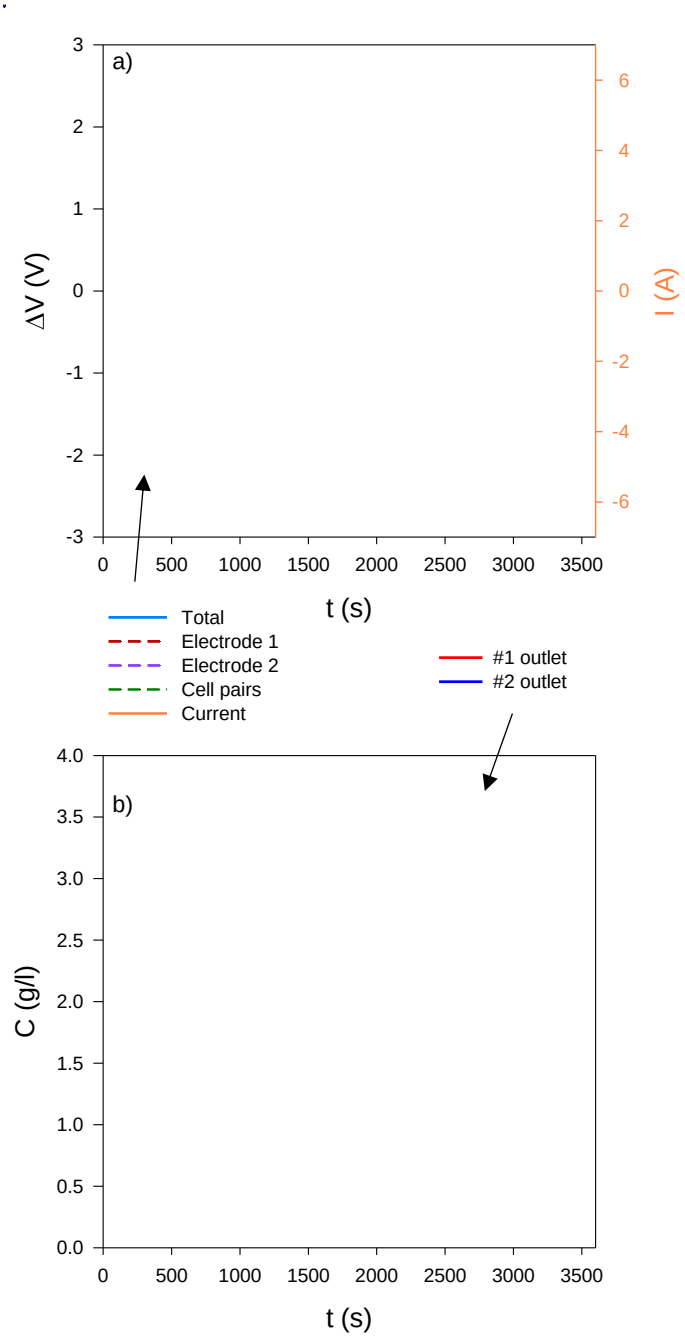

Figure 9. Simulation results of a single pass CED unit 12.5 cm wide and 80 cm long equipped with 270 µm woven spacers and Fujifilm capacitive electrodes (RC circuit properties taken from experimental results). Inlet concentration of 2 g/l, linear velocity of 2 cm/s, and ±2 V of applied voltage with polarity switches every 600 s (10 min). a) Overall, electrodes and cell pair voltage drop and current vs time, b) outlet concentrations of the two streams vs time.

Simulation results are reported in Figure 9. In particular, Figure 9 a depicts the electrical variables as a function of time. At the beginning of a cycle, electrode 2 (i.e. the pre-charged one that is rejecting cations) is actively providing a voltage in addition to the external applied voltage (of 2V) that is higher than the actual electrode 1 voltage drop. Therefore, a voltage higher than 2 V is actually applied to the cell pairs. However, during a constant voltage operation, the electrodes voltage changes, thus causing a decrease of (the absolute value of) the cell pairs voltage. Because of this phenomenon, the overall current decreases, negatively affecting the desalination rate during a cycle and thus causing the diluate outlet concentration to increase up to 0.8 g/l at the end of the cycle, as shown in Figure 9 b.

The simulated reference case of CED operation would likely present some criticalities when replicated in a real unit. Firstly, the electrode voltage goes above 1 V in the last part of each cycle, meaning that unwanted faradic reactions (i.e. water splitting) may occur at a large amount and damage at the electrodes may occur. In addition, the diluate outlet concentration increases well above the freshwater limit (set to 0.5 g/l, but usually taken even lower as a safety precaution). Therefore, with these electrodes shorter switching intervals would be required.

5.2.1 Effect of electrode capacitance on single pass CED

In order to avoid the aforementioned criticalities, maintaining the set switching interval or even extending it, the electrode should have an enhanced capacity. In this way, the electrodes voltage would grow less through time, causing a slower drop in the overall current. The latter effect would also make an impact on the diluate outlet concentration slowing down its increase. In order to numerically evaluate the improvements, the effect of electrode capacitance on process performances

has been assessed via simulations. In particular, the specific capacitance per electrode has been increased from ~ 1.2 F/cm^2 of the reference case to 2 and 3.3 F/cm^2.

Simulation results are reported in Figure 10. Comparing the reference capacitance with 2 F/cm^2, the slope of the capacitive electrodes voltage over time is already strongly reduced, thus not reaching the undesired 1 V threshold through the 600 s of constant polarity (Figure 10 a). In addition, desalination performances are also enhanced (Figure 10 b). At 2 F/cm^2, the diluate concentration goes only slightly over 0.5 g/l, achieving an acceptable result, as the outlet solution produced in the earliest part of the cycle (whose concentration was well below the limit) will be in the end mixed with the more concentrated solution exiting at the end of the cycle. Interestingly, a further increase in the capacitance up to 3.3 F/cm^2 does not provide a significant improvement to the voltage even though it still makes an impact on the outlet concentration.

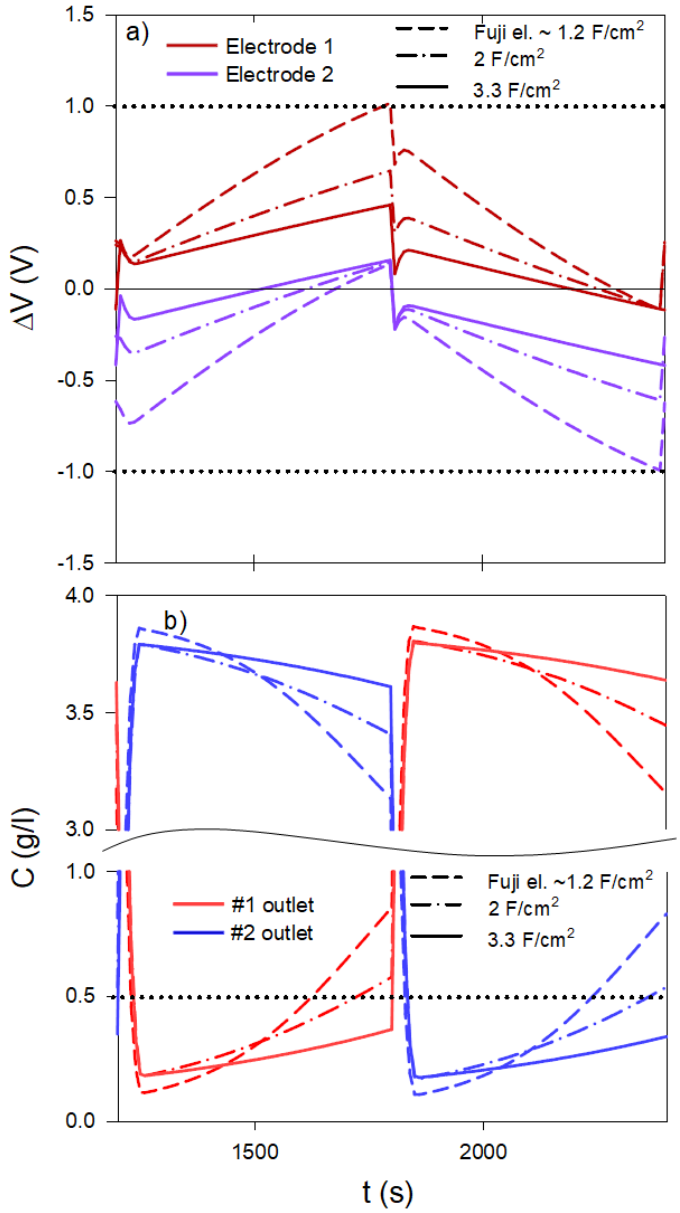

Figure 10. Comparison of different electrode capacitance (~ 1.2 , 2 and 2.5 F/cm^2) in a single pass CED unit 12.5 cm wide and 80 cm long equipped with 270 µm woven spacers and Fujifilm capacitive electrodes (RC circuit properties taken from experimental results). Inlet concentration of 2 g/l, linear velocity of 2 cm/s, and ±2 V of applied voltage with polarity switches every 600 s (10 min). a) Electrodes voltage drop vs time, b) outlet concentrations of the two streams vs time.

5.2.2 Effect of electrode resistance on single pass CED

The electrode areal resistance is another interesting parameter to analyse. The reference value of 50 Ω*cm^2 has been compared with a doubled resistance (100 Ω*cm^2) as well as with a halved one (25 Ω*cm^2), maintaining the reference value of capacitance. Figure 11 shows the results in terms of

electrode voltage and outlet concentration *vs* time. The increase in resistance causes a slight increase of the voltage as well as of the diluate concentration (due to a reduction in the stack current density). The reduction of the electrode resistance has opposite effects. Nevertheless, the influence of the electrode resistance is almost negligible , as it is relatively small compared to the average Ohmic resistance of the 12 cell pairs amounting to ~ 500 Ω*cm^2 . Consequently, a reduction in resistance does not lead to appreciable improvements of the process performance as an increase of capacitance does.

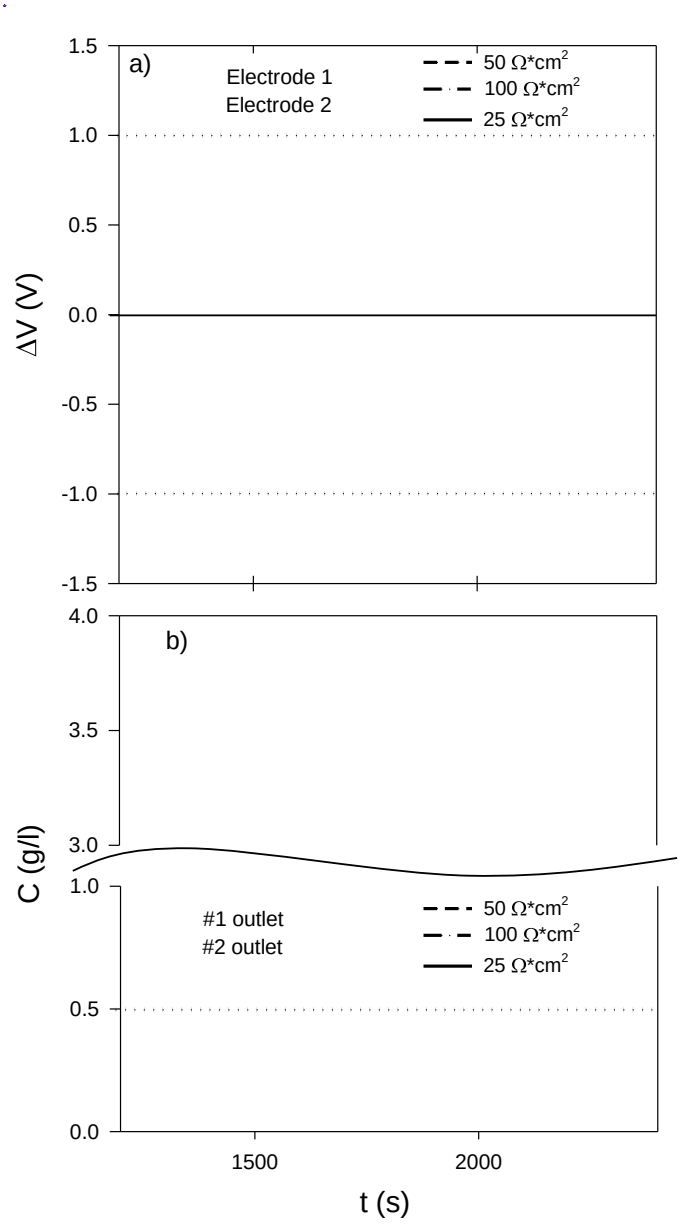

*Figure 11. Comparison of different electrode resistance (25,50 and 100 Ω*cm^2) in a single pass CED unit 12.5 cm wide and 80 cm long equipped with 270 µm woven spacers and Fujifilm capacitive electrodes (RC circuit properties taken from experimental results).*

Inlet concentration of 2 g/l, linear velocity of 2 cm/s, and ±2 V of applied voltage with polarity switches every 600 s (10 min). a) Electrodes voltage drop vs time, b) outlet concentrations of the two streams vs time.

5.2.3 Effect of the number of cell pairs

The effects of the capacitive electrode properties shown in the previous subsections are affected by the low number of cell pairs that have been simulated. In fact, an increase of the number of cell pairs can modify the impact that those properties have on the overall process. For this reason, the reference case has been replicated with a higher number of cell pairs.

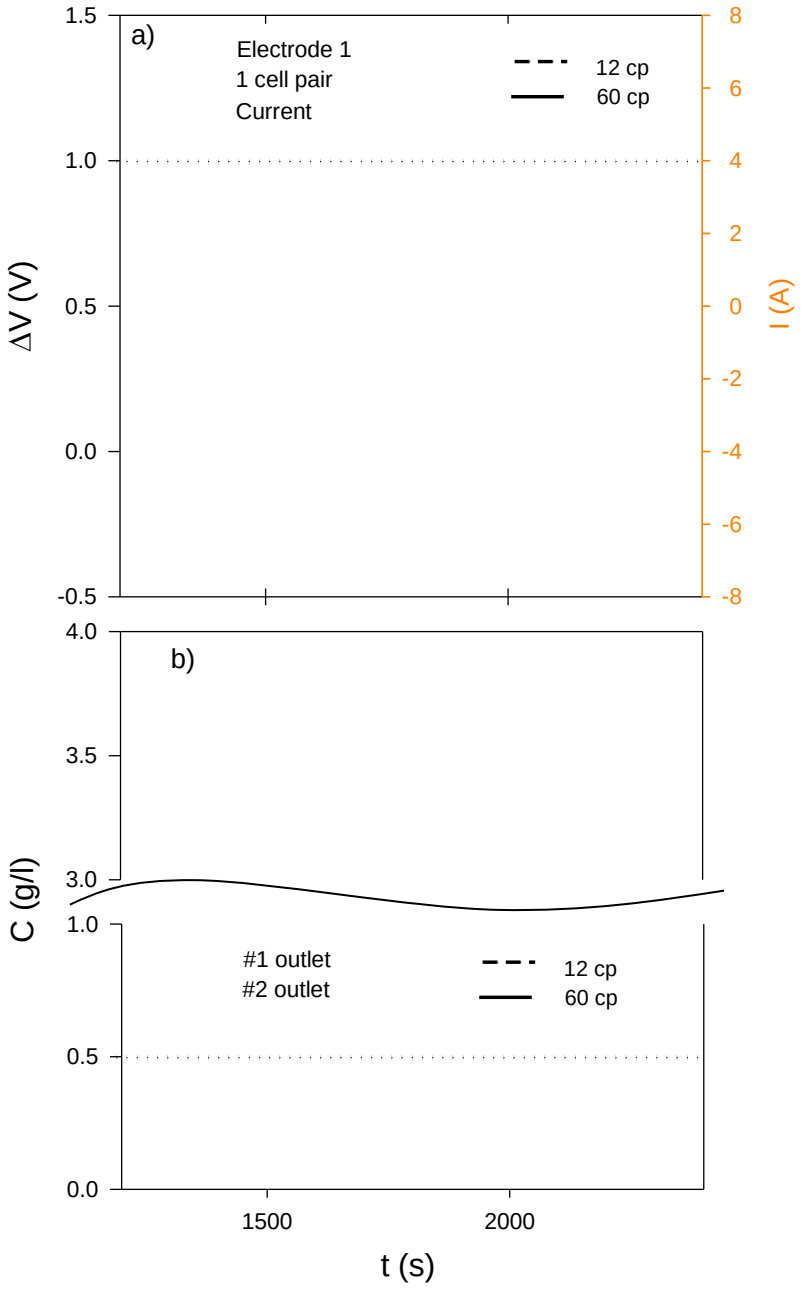

Figure 12. Effect of a different number of cell pairs (12 and 60) in a single pass CED unit 12.5 cm wide and 80 cm long equipped with 270 µm woven spacers and Fujifilm capacitive electrodes (RC circuit properties taken from experimental results). Inlet concentration of 2 g/l, linear velocity of 2 cm/s, and fixed voltage (±2 V for 12 cp, ± 9.45 V for 60 cp) with polarity switches every 600 s (10 min). a) Electrode1 and single cell pair voltage drop vs time and current vs time, b) outlet concentrations of the two streams vs time.

Figure 12 shows the comparison between the reference case and a case where 60 cell pairs have been simulated. In order to set a comparable scenario, the total voltage has been fixed in a way that, at the initial condition (i.e. at 0 s), the voltage applied at each cell pair would have been equal for the two cases. As can be seen, the main effect of increasing the number of cell pairs is a reduction of the slope of the outlet concentration *vs* time (Figure 12 b). This trend can be explained by the fact that, the more the cell pairs the smaller the electrode voltage compared to the voltage of the cell pairs. Consequently, with 60 cell pairs the electrode voltage change through time almost does not affect the current curve that becomes flatter (orange curve from Figure 12 a) and the same does the voltage drop of each cell pair (green curve from Figure 12 a). Of course, current and concentration curves would be perfectly flat for an infinite number of cell pairs. Another interesting consequence of the reduction of the current slope is the increase of the electrodes voltage slope (only V_{el}^{1} is depicted in Figure 12 a as V_{el}^{2} is qualitatively the same) as they are subjected to a higher average current. As can be deduced from previous discussions (see beginning of Section 5), the two limiting factors that cause the need to reverse polarity in CED operations are the excessive salinity of the dilute stream and the reach of the threshold value of the electrode voltage. Considering the effects on the outlet concentration and on the electrode voltage it can be observed that, increasing the number of cell pairs, a progressive shift from the concentration limiting condition to the voltage limiting condition occurs.

6. Conclusions

In this work, the feasibility of the CED process has been proven with both experiments and modelling.

A hierarchical dynamic model for the CED process has been presented for the first time. A single cell pair and the electrodes are separately described in the lowest hierarchy of the model. In particular,

capacitive electrodes are modelled as an RC circuit distributed along the direction of the flowing solution. The cell pair and capacitive electrodes are subsequently coupled in the stack model, where the overall variables and performance parameters are calculated. The stack model can be then variously arranged in the plant highest hierarchy.

A set of experiments has been performed with the aim of demonstrating the desalination capability of the CED system. In addition, an experimental characterisation of a set of capacitive electrodes has been carried out and the collected data have been used as input for the modelled RC circuit as well as to validate the CED model.

Starting from a reference case, the model has been used to assess the effect of different parameters on process performances in conditions closer to real desalination applications. By simulating the same scenario in presence of an increased capacitance, it was possible to show that the presence of a high capacitance (i.e. 2 F/cm^2) would ensure the feasibility of longer desalination cycles prior to the need of a polarity inversion, thus maintaining the electrode voltage drop below the water splitting threshold and the outlet diluate concentration below the target for a longer time. However, it has been shown that a further increase in the capacitance would unlikely lead to great improvement. A sensitivity analysis on the electrode resistance has been also carried out, demonstrating how 50 $\Omega*cm^2$ is already a low value compared to the Ohmic resistance of the membrane pile that is one order of magnitude higher. Finally, it has been shown how the increase in the number of cell pairs can change the effect of the electrodes, causing a shift in the limiting condition that controls the polarity switch frequency.

Acknowledgements

This work has been performed within the REvivED water project (Low energy solutions for drinking water production by a REvival of ElectroDialysis systems). The REvivED water project has received

funding from the European Union's Horizon 2020 research and innovation programme under Grant Agreement no. 685579 (www.revivedwater.eu).

List of symbols

A	Membrane area (m^2)
b	Membrane width (m)
C	Concentration (mol/m^3)
c_{el}	Specific capacitance (F/m^2)
D^{IEM}	Salt permeability coefficient of one IEM (m^2/s)
F	Faraday's constant (C/mol)
I	Current (A)
i	Current density (A/m^2)
J_{cond}	Conductive flux ($mol/m^2/s$)
J_{diff}^{IEM}	Diffusive flux across one IEM ($mol/m^2/s$)
L	Channel length (m)
L_p	Water permeability ($m^3/Pa/s/m^2$)
N_{pairs}	Number of cell pairs
Q	Volumetric flow rate (m^3/s)
Q_{el}	Surface charge density (C/m^2)
q_{eosm}	Electroosmotic volumetric flux ($m^3/m^2/s$)
q_{osm}^{IEM}	Osmotic volumetric flux across one IEM ($m^3/m^2/s$)
q_w	Total water volumetric flux ($m^3/m^2/s$)
R	Areal electrical resistance (Ωm^2)
R_G	Universal gas constant (J/mol/K)
$t^{counter}$	Counter-ion transport number in the membrane
t	Time (s)
V_{tot}	Overall voltage drop (V)
V_{cp}	Voltage drop over one cell pair (V)
${V_{el}}^{j}$	Electrode j voltage drop (V)
V_{10cp}	Voltage drop over 10 cell pairs (V)

w	Total water transport number
x	Coordinate in the direction of the main flow

Greek letters

α	Permselectivity
δ	Channel thickness (m)
η	Non-Ohmic voltage drop (V)
π	Osmotic pressure (Pa)

Subscripts and superscripts

AEM	Anion-exchange membrane
C	Concentrate
CEM	Cation-exchange membrane
D	Dilute
el	Capacitive electrode
IEM	Ion-exchange membrane
int	Value at the membrane -solution interface, solution side

References

[1] H. Strathmann, Electrodialysis, a mature technology with a multitude of new applications, Desalination. 264 (2010) 268–288. doi:10.1016/j.desal.2010.04.069.

[2] A. Campione, L. Gurreri, M. Ciofalo, G. Micale, A. Tamburini, A. Cipollina, Electrodialysis for water desalination: A critical assessment of recent developments on process fundamentals, models and applications, Desalination. 434 (2018) 121–160. doi:10.1016/j.desal.2017.12.044.

[3] A.H. Galama, M. Saakes, H. Bruning, H.H.M. Rijnaarts, J.W. Post, Seawater predesalination with electrodialysis, Desalination. 342 (2014) 61–69. doi:10.1016/j.desal.2013.07.012.

[4] B. Van der Bruggen, Advances in electrodialysis for water treatment, in: A. Basile, A. Cassano, N.K. Rastogi (Eds.), Adv. Membr. Technol. Water Treat. Mater. Process. Appl., Woodhead Publishing, 2015: pp. 185–203. doi:10.1016/B978-1-78242-121-4.00006-X.

[5] J.H. Barber, R. MacDonald, H. Yang, W. Lu, Capacitive carbon electrodes for electrodialysis reversal applications, in: American Water Works Association, 2014.

[6] C. Wei, Y. Du, W. Cai, R. Xiong, L. Cao, Non-faraday based systems, devices and methods for removing ionic species from liquid, US20110042219A1, 2011.

[7] D.A. Vermaas, S. Bajracharya, B.B. Sales, M. Saakes, B. Hamelers, K. Nijmeijer, Clean energy generation using capacitive electrodes in reverse electrodialysis, Energy Environ. Sci. 6 (2013) 643–651. doi:10.1039/C2EE23562E.

[8] P. Ratajczak, M.E. Suss, F. Kaasik, F. Béguin, Carbon electrodes for capacitive technologies, Energy Storage Mater. 16 (2019) 126–145. doi:10.1016/j.ensm.2018.04.031.

[9] P.M. Biesheuvel, M.Z. Bazant, Nonlinear dynamics of capacitive charging and desalination by porous electrodes, Phys. Rev. E. 81 (2010) 031502. doi:10.1103/PhysRevE.81.031502.

[10] M.E. Suss, T.F. Baumann, M.A. Worsley, K.A. Rose, T.F. Jaramillo, M. Stadermann, J.G. Santiago, Impedance-based study of capacitive porous carbon electrodes with hierarchical and bimodal porosity, J. Power Sources. 241 (2013) 266–273. doi:10.1016/J.JPOWSOUR.2013.03.178.

[11] G. Wang, L. Zhang, J. Zhang, A review of electrode materials for electrochemical supercapacitors, Chem. Soc. Rev. 41 (2012) 797–828. doi:10.1039/C1CS15060J.

[12] E. Frackowiak, F. Béguin, Carbon materials for the electrochemical storage of energy in capacitors, Carbon N. Y. 39 (2001) 937–950. doi:10.1016/S0008-6223(00)00183-4.

[13] Y. Ding, J. Zhu, C. Wang, B. Dai, Y. Li, Y. Qin, F. Xu, Q. Peng, Z. Yang, J. Bai, W. Cao, Y. Yuan, Y. Li, Multifunctional three-dimensional graphene nanoribbons composite sponge, Carbon N. Y. 104 (2016) 133–140. doi:10.1016/J.CARBON.2016.03.058.

[14] E. Castillo-Martínez, J. Carretero-González, J. Sovich, M.D. Lima, High temperature structural transformations of few layer graphene nanoribbons obtained by unzipping carbon nanotubes, J. Mater. Chem. A. 2 (2014) 221–228. doi:10.1039/C3TA13292G.

[15] X. Zhou, L. Yu, X.-Y. Yu, X.W.D. Lou, Encapsulating Sn Nanoparticles in Amorphous Carbon Nanotubes for Enhanced Lithium Storage Properties, Adv. Energy Mater. 6 (2016) 1601177. doi:10.1002/aenm.201601177.

[16] G. Xiong, P. He, Z. Lyu, T. Chen, B. Huang, L. Chen, T.S. Fisher, Bioinspired leaves-on-branchlet hybrid carbon nanostructure for supercapacitors, Nat. Commun. 9 (2018) 790. doi:10.1038/s41467-018-03112-3.

[17] E.S. Snow, F.K. Perkins, E.J. Houser, S.C. Badescu, T.L. Reinecke, Chemical Detection with a Single-Walled Carbon Nanotube Capacitor, Science (80-.). 307 (2005) 1942–1945. doi:10.1126/science.1109128.

[18] C. Portet, G. Yushin, Y. Gogotsi, Electrochemical performance of carbon onions, nanodiamonds, carbon black and multiwalled nanotubes in electrical double layer capacitors, Carbon N. Y. 45 (2007) 2511–2518. doi:10.1016/J.CARBON.2007.08.024.

[19] M.E. Plonska-Brzezinska, L. Echegoyen, Carbon nano-onions for supercapacitor electrodes: recent developments and applications, J. Mater. Chem. A. 1 (2013) 13703. doi:10.1039/c3ta12628e.

[20] J. García-Martínez, K. Li, Mesoporous Zeolites, Wiley-VCH Verlag GmbH & Co. KGaA, Weinheim, Germany, 2015. doi:10.1002/9783527673957.

[21] N. Boukmouche, N. Azzouz, L. Bouchama, J.P. Chopart, Y. Bouznit, Activated carbon derived from marine Posidonia Oceanica for electric energy storage, Arab. J. Chem. 7 (2014) 347–354. doi:10.1016/j.arabjc.2012.12.010.

[22] F. Béguin, V. Presser, A. Balducci, E. Frackowiak, Carbons and Electrolytes for Advanced Supercapacitors, Adv. Mater. 26 (2014) 2219–2251. doi:10.1002/adma.201304137.

[23] H.F. Stoeckli, F. Kraehenbuehl, The external surface of microporous carbons, derived from adsorption and immersion studies, Carbon N. Y. 22 (1984) 297–299. doi:10.1016/0008-6223(84)90174-X.

[24] T. Alencherry, N. A.R., S. Ghosh, J. Daniel, V. R., Effect of increasing electrical conductivity and hydrophilicity on the electrosorption capacity of activated carbon electrodes for capacitive deionization, Desalination. 415 (2017) 14–19. doi:10.1016/J.DESAL.2017.04.001.

[25] L. Zou, G. Morris, D. Qi, Using activated carbon electrode in electrosorptive deionisation of brackish water, Desalination. 225 (2008) 329–340. doi:10.1016/J.DESAL.2007.07.014.

[26] C.-H. Hou, C.-Y. Huang, A comparative study of electrosorption selectivity of ions by activated carbon electrodes in capacitive deionization, Desalination. 314 (2013) 124–129. doi:10.1016/J.DESAL.2012.12.029.

[27] J.Y. Hwang, M. Li, M.F. El-Kady, R.B. Kaner, Next-Generation Activated Carbon Supercapacitors: A Simple Step in Electrode Processing Leads to Remarkable Gains in Energy Density, Adv. Funct. Mater. 27 (2017) 1605745. doi:10.1002/adfm.201605745.

[28] M. Olivares-Marín, J.A. Fernández, M.J. Lázaro, C. Fernández-González, A. Macías-García, V. Gómez-Serrano, F. Stoeckli, T.A. Centeno, Cherry stones as precursor of activated carbons for supercapacitors, Mater. Chem. Phys. 114 (2009) 323–327. doi:10.1016/J.MATCHEMPHYS.2008.09.010.

[29] I. Villar, S. Roldan, V. Ruiz, M. Granda, C. Blanco, R. Menéndez, R. Santamaría, Capacitive Deionization of NaCl Solutions with Modified Activated Carbon Electrodes †, Energy & Fuels. 24 (2010) 3329–3333. doi:10.1021/ef901453q.

[30] C. Vix-Guterl, E. Frackowiak, K. Jurewicz, M. Friebe, J. Parmentier, F. Béguin, Electrochemical energy storage in ordered porous carbon materials, Carbon N. Y. 43 (2005) 1293–1302. doi:10.1016/J.CARBON.2004.12.028.

[31] A.G. Pandolfo, A.F. Hollenkamp, Carbon properties and their role in supercapacitors, J. Power Sources. 157 (2006) 11–27. doi:10.1016/J.JPOWSOUR.2006.02.065.

[32] F. Liu, O. Coronell, D.F. Call, Electricity generation using continuously recirculated flow electrodes in reverse electrodialysis, J. Power Sources. 355 (2017) 206–210. doi:10.1016/J.JPOWSOUR.2017.04.061.

[33] J.M. Paz-Garcia, O. Schaetzle, P.M. Biesheuvel, H.V.M. Hamelers, Energy from CO2 using capacitive electrodes – Theoretical outline and calculation of open circuit voltage, J. Colloid Interface Sci. 418 (2014) 200–207. doi:10.1016/J.JCIS.2013.11.081.

[34] D. Brogioli, Extracting Renewable Energy from a Salinity Difference Using a Capacitor, Phys. Rev. Lett. 103 (2009) 058501. doi:10.1103/PhysRevLett.103.058501.

[35] Y.A.C. Jande, W.S. Kim, Desalination using capacitive deionization at constant current, Desalination. 329 (2013) 29–34. doi:10.1016/J.DESAL.2013.08.023.

[36] Y. Salamat, C.H. Hidrovo, A parametric study of multiscale transport phenomena and performance characteristics of capacitive deionization systems, Desalination. 438 (2018) 24–36. doi:10.1016/J.DESAL.2018.03.022.

[37] Z. Chen, H. Zhang, C. Wu, L. Luo, C. Wang, S. Huang, H. Xu, A study of the effect of carbon characteristics on capacitive deionization (CDI) performance, Desalination. 433 (2018) 68–74. doi:10.1016/J.DESAL.2017.11.036.

[38] O.N. Demirer, R.M. Naylor, C.A. Rios Perez, E. Wilkes, C. Hidrovo, Energetic performance optimization of a capacitive deionization system operating with transient cycles and brackish water, Desalination. 314 (2013) 130–138. doi:10.1016/J.DESAL.2013.01.014.

[39] J. Ma, C. He, D. He, C. Zhang, T.D. Waite, Analysis of capacitive and electrodialytic contributions to water desalination by flow-electrode CDI, Water Res. 144 (2018) 296–303. doi:10.1016/J.WATRES.2018.07.049.

[40] H.J. Lee, F. Sarfert, H. Strathmann, S.H. Moon, Designing of an electrodialysis desalination plant, Desalination. 142 (2002) 267–286. doi:10.1016/S0011-9164(02)00208-4.

[41] M. Sadrzadeh, A. Kaviani, T. Mohammadi, Mathematical modeling of desalination by electrodialysis, Desalination. 206 (2007) 538–546. doi:10.1016/j.desal.2006.04.062.

[42] G. Kraaijeveld, V. Sumberova, S. Kuindersma, H. Wesselingh, Modelling electrodialysis using the Maxwell-Stefan description, Chem. Eng. J. Biochem. Eng. J. 57 (1995) 163–176. doi:10.1016/0923-0467(94)02940-7.

[43] R.K. McGovern, S.M. Zubair, J.H. Lienhard V, The cost effectiveness of electrodialysis for diverse salinity applications, Desalination. 348 (2014) 57–65. doi:10.1016/j.desal.2014.06.010.

[44] M. Fidaleo, M. Moresi, Optimal strategy to model the electrodialytic recovery of a strong electrolyte, J. Memb. Sci. 260 (2005) 90–111. doi:10.1016/j.memsci.2005.01.048.

[45] N.C. Wright, S.R. Shah, S.E. Amrose, A.G. Winter, A robust model of brackish water electrodialysis desalination with experimental comparison at different size scales, Desalination. 443 (2018) 27–43. doi:10.1016/J.DESAL.2018.04.018.

[46] Z. Zourmand, F. Faridirad, N. Kasiri, T. Mohammadi, Mass transfer modeling of desalination through an electrodialysis cell, Desalination. 359 (2015) 41–51. doi:10.1016/j.desal.2014.12.008.

[47] K. Tado, F. Sakai, Y. Sano, A. Nakayama, An analysis on ion transport process in electrodialysis desalination, Desalination. 378 (2016) 60–66. doi:10.1016/j.desal.2015.10.001.

[48] R. Enciso, J.A. Delgadillo, O. Domínguez, I. Rodríguez-Torres, Analysis and validation of the hydrodynamics of an electrodialysis cell using computational fluid dynamics, Desalination. 408 (2017) 127–132. doi:10.1016/j.desal.2017.01.015.

[49] M. Tedesco, H.V.M. Hamelers, P.M. Biesheuvel, Nernst-Planck transport theory for (reverse) electrodialysis: I. Effect of co-ion transport through the membranes, J. Memb. Sci. 510 (2016) 370–381.

[50] M. Tedesco, H.V.M. Hamelers, P.M. Biesheuvel, Nernst-Planck transport theory for (reverse) electrodialysis: II. Effect of water transport through ion-exchange membranes, J. Memb. Sci. 531 (2017) 172–182. doi:10.1016/j.memsci.2017.02.031.

[51] Y. Tanaka, Concentration polarization in ion-exchange membrane electrodialysis: The events arising in an unforced flowing solution in a desalting cell, J. Memb. Sci. 244 (2004) 1–16. doi:10.1016/j.memsci.2004.02.041.

[52] J.A. Wesselingh, P. Vonk, G. Kraaijeveld, Exploring the Maxwell-Stefan description of ion exchange, Chem.

Eng. J. Biochem. Eng. J. 57 (1995) 75–89. doi:10.1016/0923-0467(94)02932-6.

[53] P.N. Pintauro, D.N. Bennion, Mass transport of electrolytes in membranes. 1. Development of mathematical transport model, Ind. Eng. Chem. Fundam. 23 (1984) 230–234.

[54] M. Andelman, Flow through capacitor basics, Sep. Purif. Technol. 80 (2011) 262–269. doi:10.1016/j.seppur.2011.05.004.

[55] Y. Qu, P.G. Campbell, L. Gu, J.M. Knipe, E. Dzenitis, J.G. Santiago, M. Stadermann, Energy consumption analysis of constant voltage and constant current operations in capacitive deionization, Desalination. 400 (2016) 18–24. doi:10.1016/J.DESAL.2016.09.014.

[56] A. Hemmatifar, M. Stadermann, J.G. Santiago, Two-Dimensional Porous Electrode Model for Capacitive Deionization, J. Phys. Chem. C. 119 (2015) 24681–24694. doi:10.1021/acs.jpcc.5b05847.

[57] J. Newman, W. Tiedemann, Porous-electrode theory with battery applications, AIChE J. 21 (1975) 25–41. doi:10.1002/aic.690210103.

[58] A.M. Johnson, J. Newman, Desalting by Means of Porous Carbon Electrodes, J. Electrochem. Soc. 118 (1971) 510. doi:10.1149/1.2408094.

[59] J.S. Newman, Electrochemical Systems, second, Prentice Hall, Englewood Cliffs, 1991.

[60] P.M. Biesheuvel, Y. Fu, M.Z. Bazant, Diffuse charge and Faradaic reactions in porous electrodes, Phys. Rev. E. 83 (2011) 061507. doi:10.1103/PhysRevE.83.061507.

[61] M. La Cerva, M. Di Liberto, L. Gurreri, A. Tamburini, A. Cipollina, G. Micale, M. Ciofalo, Coupling CFD with simplified 1-D models to predict the performance of reverse electrodialysis stacks, J. Memb. Sci. 541 (2017) 595–610. doi:10.1016/j.memsci.2017.07.030.

[62] S. Pawlowski, V. Geraldes, J.G. Crespo, S. Velizarov, Computational fluid dynamics (CFD) assisted analysis of profiled membranes performance in reverse electrodialysis, J. Memb. Sci. 502 (2016) 179–190.

[63] M. Tedesco, A. Cipollina, A. Tamburini, I.D.L. Bogle, G. Micale, A simulation tool for analysis and design of reverse electrodialysis using concentrated brines, Chem. Eng. Res. Des. 93 (2015) 441–456. doi:10.1016/j.cherd.2014.05.009.

[64] K.M. Chehayeb, D.M. Farhat, K.G. Nayar, J.H. Lienhard, Optimal design and operation of electrodialysis for brackish-water desalination and for high-salinity brine concentration, Desalination. 420 (2017) 167–182. doi:10.1016/j.desal.2017.07.003.

[65] N.A.A. Qasem, B.A. Qureshi, S.M. Zubair, Improvement in design of electrodialysis desalination plants by considering the Donnan potential, Desalination. 441 (2018) 62–76. doi:10.1016/j.desal.2018.04.023.

[66] B.A. Qureshi, S.M. Zubair, Design of electrodialysis desalination plants by considering dimensionless groups and variable equivalent conductivity, Desalination. 430 (2018) 197–207. doi:10.1016/j.desal.2017.12.030.

[67] A. Campione, A. Cipollina, I.D.L. Bogle, L. Gurreri, A. Tamburini, M. Tedesco, G. Micale, A hierarchical model for novel schemes of electrodialysis desalination, Desalin. (under Rev. (2019).

[68] R. de Levie, On porous electrodes in electrolyte solutions: I. Capacitance effects, Electrochim. Acta. 8 (1963) 751–780. doi:10.1016/0013-4686(63)80042-0.

[69] R. Kötz, M. Carlen, Principles and applications of electrochemical capacitors, Electrochim. Acta. 45 (2000) 2483–2498. doi:10.1016/S0013-4686(00)00354-6.

[70] P.M. Biesheuvel, H.V.M. Hamelers, M.E. Suss, Theory of Water Desalination by Porous Electrodes with Immobile Chemical Charge, Colloids Interface Sci. Commun. 9 (2015) 1–5. doi:10.1016/J.COLCOM.2015.12.001.

[71] E.N. Guyes, A.N. Shocron, A. Simanovski, P.M. Biesheuvel, M.E. Suss, A one-dimensional model for water desalination by flow-through electrode capacitive deionization, Desalination. 415 (2017) 8–13. doi:10.1016/J.DESAL.2017.03.013.

[72] L. Gurreri, A. Tamburini, A. Cipollina, G. Micale, M. Ciofalo, CFD prediction of concentration polarization phenomena in spacer-filled channels for reverse electrodialysis, J. Memb. Sci. 468 (2014) 133–148. doi:10.1016/j.memsci.2014.05.058.

[73] L. Gurreri, A. Tamburini, A. Cipollina, G. Micale, M. Ciofalo, Flow and mass transfer in spacer-filled channels for reverse electrodialysis: a CFD parametrical study, J. Memb. Sci. 497 (2016) 300–317. doi:10.1016/j.memsci.2015.09.006.

[74] L. Gurreri, M. Ciofalo, A. Cipollina, A. Tamburini, W. Van Baak, G. Micale, CFD modelling of profiled-membrane channels for reverse electrodialysis, Desalin. Water Treat. 55 (2015) 1–20. doi:10.1080/19443994.2014.940651.

[75] L. Gurreri, A. Tamburini, A. Cipollina, G. Micale, M. Ciofalo, Pressure drop at low reynolds numbers in woven-spacer-filled channels for membrane processes: CFD prediction and experimental validation, Desalin. Water Treat. 61 (2017) 170–182. doi:10.5004/dwt.2016.11279.

[76] D.L. Chapman, LI. A contribution to the theory of electrocapillarity, London, Edinburgh, Dublin Philos. Mag. J. Sci. 25 (1913) 475–481. doi:10.1080/14786440408634187.